Invisible fat on CT: making it visible by MRI

Emre Ünal
Ali Devrim Karaosmanoğlu
Deniz Akata
Mustafa Nasuh Özmen
Muşturay Karçaaltıncaba

ABSTRACT
Presence of fat in a lesion significantly narrows the differential diagnosis. Small quantities of macroscopic fat and intracellular fat are invisible on computed tomography (CT) and ultrasonography. Magnetic resonance imaging (MRI) can reveal any fatty change in a lesion and can also differentiate macroscopic fat from intracellular and intravoxel fat. Hypodensity on CT may be a sign of invisible fat and MRI can help to diagnose even minute amounts of fat in liver, pancreas, adrenal, musculoskeletal, and omental pseudolesions and lesions. This article will review the superiority of MRI over CT in demonstrating fat in abdominal lesions.

Computed tomography (CT) can be a very sensitive modality to detect small subcentimeter lesions with its high spatial resolution (1, 2). However, despite its superiority in detection of these small lesions, further characterization may be difficult or even impossible in an important percentage of the patients (1–3). This is particularly more important in patients with history of cancer as the detection of a new lesion in the interval follow-up is always suspicious for metastatic disease, which has important implications in the clinical decision-making process (1, 4). In these clinical scenarios, the detection of fat in these lesions may be helpful, as this finding is an important clue in narrowing the list of differential diagnosis.

In this article, we review the diagnostic role of magnetic resonance imaging (MRI) in the detection of fat, which may be difficult, or sometimes even impossible, to detect with CT. We also present challenging cases to further support the role of MRI.

Fat detection techniques

Inversion recovery imaging

Short tau inversion recovery (STIR) sequence is based on T1 differences of the protons. Fat has a short T1 value than water. STIR, which is usually performed with a fast spin-echo sequence, starts with initial 180° preparation pulse, followed by a 90° excitation pulse. There is a specific time interval between preparation and excitation pulses referred to as the inversion time (TI). Specific TI is selected such that net magnetization vector of fat protons stops at the null point, so that there is no signal from the fat protons. The TI for fat suppression is approximately 130–170 ms at 1.5 T (5). At high-field-strength magnets, the TI increases proportional to increased T1 value.

STIR technique has a low sensitivity to magnetic field inhomogeneities and can be used with low-field-strength magnets (5, 6). STIR is primarily used to reveal fluid, not fat. Short TI, which corresponds to short T1- and T2-weighted imaging, enhances tissues that have more fluid content (i.e., tumors). However, signal from protons that have short TI similar to fat, such as subacute hemorrhage, gadolinium, and viscous fluid, are also adversely suppressed (6, 7).

Frequency selective fat suppression

Chemical shift selective (CHESS) imaging (also known as fat-sat) depends on the idea of exciting only fat protons with a narrow-band pulse, dephase the signal with added spoiler gradients, and then immediately continue imaging sequence (6, 7). Because suppression is limited to fat, gadolinium can be used and sequence is not affected by the tissue

From the Department of Radiology (E.Ü., A.D.K., D.A., M.N.Ö., M.K. ✉ *musturayk@yahoo.com*), Hacettepe University School of Medicine, Ankara, Turkey; the Department of Radiology (E.Ü.), Zonguldak Atatürk State Hospital, Zonguldak, Turkey.
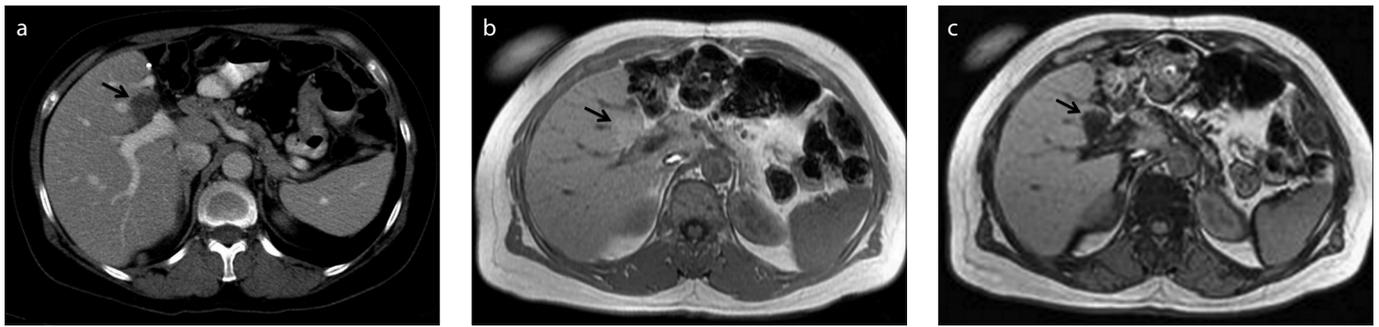
Figure 1. a–c. A 50-year-old female patient with gastric carcinoma. Follow-up contrast-enhanced axial CT image **(a)** shows a new hypodense lesion *(arrow)* suspicious for metastasis in a typical location for focal fat. In-phase **(b)** and opposed-phase **(c)** MRI demonstrate fat content *(arrow)* that is invisible on CT.

T1 value, unlike STIR. However, using spoiler gradients makes CHESS imaging sensitive to magnetic field inhomogeneities (6, 7). Therefore, this technique should be used with high-field-strength magnets.

In-phase and opposed-phase imaging

This technique depends on precessional frequency difference of fat and water protons. Immediately after the radiofrequency (RF) pulse, fat and water protons will be in the same phase (in-phase). However, since fat precesses slower than water, after a specific time water protons will complete a 360° rotation unlike fat protons, which will only be able to complete a 180° rotation. Thus fat and water protons will be opposed phase to each other. This phase cycling corresponds to 2.2 ms intervals (4.4 ms for in-phase and 2.2 ms for opposed-phase) at 1.5 T (7, 8). The opposed-phase images are differentiated from in-phase images by the characteristic India ink artifact. At the interface between fat and nonfat tissue (fat-muscle or fat-abdominal solid organ), equal number of fat and water protons cause signal loss outlining the abdominal organs and musculature (8).

In-phase and opposed-phase imaging is an irreplaceable sequence since it

demonstrates microscopic (intracellular) fat unlike other techniques. Thus, intracellular lipid-containing lesions such as focal hepatic steatosis, hepatocellular, and adrenal adenomas can easily be diagnosed (8, 9).

SPIR and SPAIR

Spectral presaturation with inversion recovery (SPIR) and spectral presaturation attenuated inversion recovery (SPAIR) are obtained by both selective excitation of the fat and T1 relaxation techniques. Initially an inversion pulse is applied. Unlike STIR, it is designated to excite only fat protons. Subsequently, as the fat protons pass through the null point, a conventional MRI sequence is started. Because the inversion pulse is specific to fat protons, tissues that have similar T1 values with fat, such as contrast-enhanced tissues, will not be suppressed, unlike STIR.

SPIR and SPAIR are differentiated by the flip angle of the initial inversion pulse. RF pulses of 180° and slightly greater than 90° are used in SPAIR and SPIR techniques, respectively (7). Avoiding 180° pulse in SPIR technique saves time; however, SPIR is sensitive to magnetic field inhomogeneity (7).

Dixon technique

The principle of Dixon technique depends on in-phase and opposed-phase imaging (10). In the two-point Dixon method, four sets of images are acquired; first two are the aforementioned in-phase and opposed-phase images. The last two images are water-only and fat-only images reconstructed by adding and subtracting in- and opposed-phase images, respectively. However, magnetic field inhomogeneity, which is ignored in two-point Dixon imag-

ing, leads to calculation and phase errors. To overcome this drawback an extra image set is acquired in modified Dixon imaging (three-point Dixon). The third set of images is obtained at the next in-phase. Thus, two sets of in-phase images are achieved in three-point Dixon technique and they should have the same phase behavior. Any differences between these two in-phase images can be attributed to phase errors and corrected (7, 11).

Water excitation

Due to precessional frequency difference of fat and water protons, fat suppression can be achieved by exciting only the water protons with the adjusted RF pulses (every 2.2 ms at 1.5 T). This technique is less sensitive to magnetic field inhomogeneity than CHESS and SPIR.

Clinical applications

Liver

Macroscopic fat containing liver lesions, such as lipomas, can easily be diagnosed on CT by its characteristic findings. However, in some cases the CT findings can be inconclusive and confusing. Among the most confusing liver lesions on CT are the focal fat sparing and deposition in the liver parenchyma. Although the diagnosis of these abnormalities might be easier in typical locations such as near the gallbladder fossa, medial segment of the left hepatic lobe, or close to the falciform ligament (12, 13), in atypical locations and in case of unconventional morphology, the diagnosis can be difficult. Focal steatotic changes are more and more commonly seen in oncologic patients due to complex and prolonged chemotherapy (14). Therefore, in case a new liver lesion detected in the follow-up of these patients,

---

Main points

- Presence of fat in a lesion significantly limits the differential diagnosis.
- Focal benign fat deposition in liver and pancreas may mimic metastasis, particularly in patients with malignancy.
- A hypodense lesion without negative HU on CT can contain fat.
- Small amounts of fat may be invisible on CT but can be detected by MRI using in- and opposed-phase imaging.
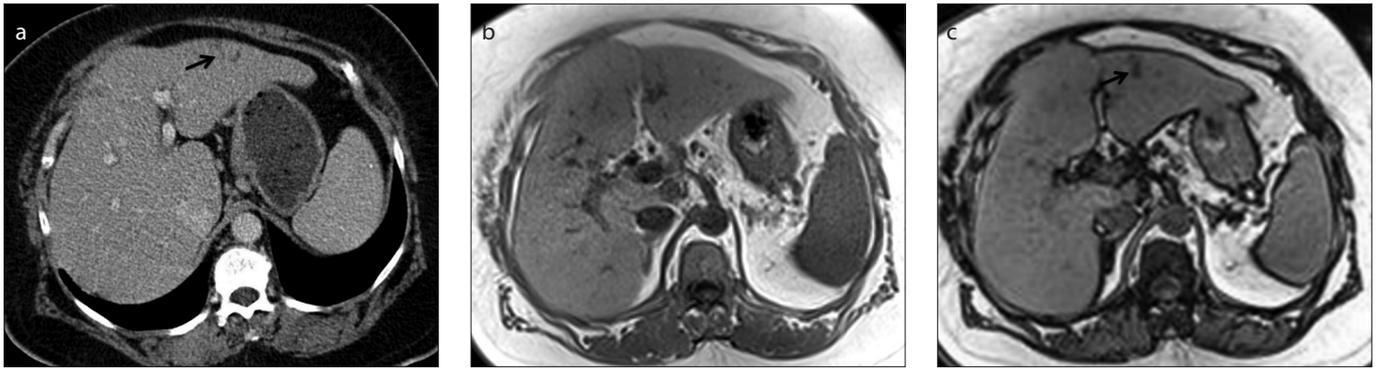
Figure 2. a–c. A 64-year-old female patient with colon carcinoma. Contrast-enhanced axial CT image **(a)** shows a new nonspecific hypodense lesion *(arrow)* in left lobe of the liver. In-phase **(b)** and opposed-phase **(c)** MRI demonstrate focal fat infiltration *(arrow)* invisible on CT.
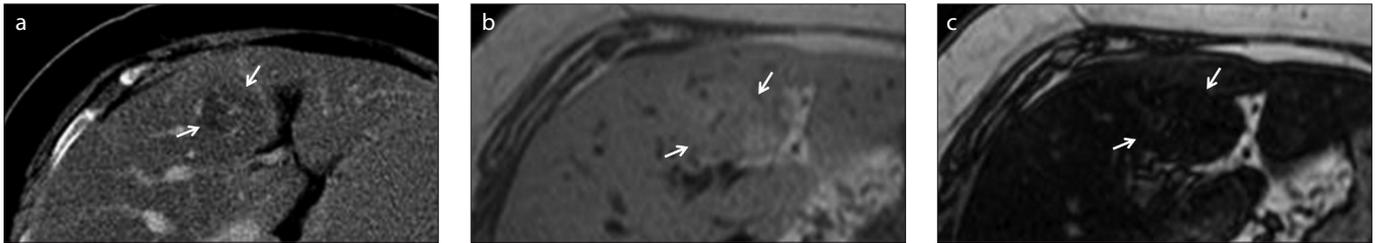

Figure 3. a–c. A 68-year-old female patient with breast carcinoma. Contrast-enhanced axial CT image **(a)** shows a new hypodense lesion *(arrows)* thought to be a metastasis in a steatotic liver. In-phase **(b)** and opposed-phase **(c)** MRI reveal liver steatosis along with focal hypersteatosis *(arrows)*.
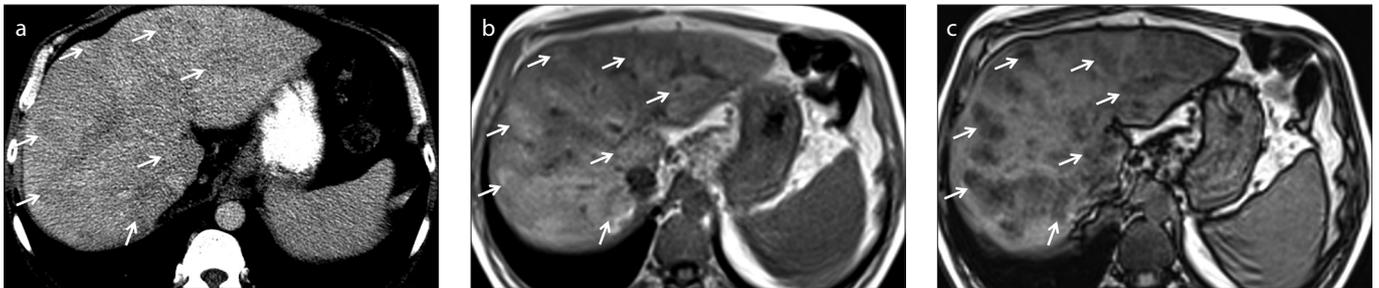

Figure 4. a–c. A 50-year-old male patient with elevated liver enzymes. Unenhanced axial CT image **(a)** shows subtle parenchymal heterogeneity due to nonspecific hypodense areas *(arrows)*. In-phase **(b)** and opposed-phase **(c)** MRI demonstrate perivenous fat infiltration *(arrows)* that is not visible on CT.

focal fatty change should be considered, especially if it is detected in conventional locations (Fig. 1). In such cases, MRI should be performed to detect the focal fatty changes and intracellular fat, which can be impossible to detect on CT (Figs. 2–4).

Another challenging liver lesion is the hepatic adenoma. Intracellular fat content was reported in 35%–77% of cases on in-phase and opposed-phase MRI (15, 16). Even more confusingly, hepatic adenomas can also demonstrate FDG avidity and can easily be reported as a metastatic focus in the liver of oncology patients. In such cases in-phase and opposed-phase MRI might reveal the fat content that is invisible on CT and prevent diagnostic confusion and invasive procedures, as well as the emotional stress on the patient (Fig. 5).

Portal vein thrombosis may cause parenchymal fatty replacement (17). CT findings may be subtle or questionable for a mass. MRI should be preferred to show fatty parenchymal changes, which cannot be diagnosed by CT (Fig. 6).

Small foci of fat can also be visualized in angiomyolipoma, liposarcoma, lipoma, and hydatid cysts in the liver (9, 16). Especially in patients with hydatid liver disease, the detection of fat globules in the cyst is an extremely important finding, which might indicate the presence of an abnormal communication between the hydatid cyst and the biliary system. As the presence of this abnormal communication will preclude the patient from conventional percutaneous therapy, they should be meticulously searched for in these patients. They can also

be visualized in CT but might be difficult to detect, especially to an inexperienced eye, when they are small in size (18) (Fig. 7).

Adrenal gland

Adrenal adenomas are the most common adrenal lesions, found in 9% of the general population (7, 19, 20). Adrenal adenoma is differentiated from other pathologies mostly by the presence of intracellular fat, which cannot be visually detected on CT. For quantitative evaluation of these adenomas by CT, an initial unenhanced CT imaging is acquired. If the attenuation value of the lesion is less than 10 HU, a diagnosis of lipid-rich adrenal adenoma can be made with a high level of confidence. If the attenuation value is greater than 10 HU as seen in case of lipid-poor adrenal adenomas, then, a multiple phase CT

study with intravenous contrast administration should be planned (20).

Alternatively, MRI with in-phase and opposed-phase imaging can also be used to detect the intracellular fat content without any use of radiation or intravenous contrast material.

In addition, hepatocellular carcinoma metastases to adrenal glands may contain fat and should not be confused with adenoma (21). Invisible fat in a metastatic lesion can mimic cystic-necrotic degeneration of an adrenal mass on CT and distinction is only possible by MRI (Fig. 8).

Pancreas

Diffuse fatty infiltration of the pancreatic parenchyma is a common imaging finding, particularly in elderly patients. In typical cases, it can generally be easily diagnosed by ultrasonography and CT. However, the focal fatty infiltration of the pancreatic parenchyma, rather than the diffuse pattern, may pose significant diagnostic difficulty (22, 23). In some cases, focal fat deposition in the pancreas may mimic a pancreatic malignancy, mostly an adenocarcinoma of the pancreas, and differentiation of these two completely different entities might be difficult, or even impossible, on CT (Fig. 9).

In case of pancreatic head neoplasia, the absence of pancreatic duct and common bile duct dilatation may be an important diagnostic clue exclude a pancreatic mass; however, it is also very-well known that pancreatic adenocarcinomas of small size may not cause any of the classical findings. The diagnosis by CT might be even more challenging in these cases, and MRI with the application of in-phase and opposed-phase imaging might preclude the patient from a major surgery, with potential significant morbidity and mortality.

Pancreatic lymphangioma is another clinical entity that may underline the importance of MRI. Pancreatic lymphangioma is a rare benign tumor that presents as a cystic mass (24, 25). Differentiation from malignant cystic carcinoma is challenging unless fluid-fluid level or fat component is revealed. However, fluid-fluid level may also be seen with metastatic pancreatic masses as a result of hemorrhage (26). Thus, the key to diagnose lymphangioma is to reveal the fat content, which is frequently invisible on CT (Fig. 10).

Primary pancreatic lymphoma, a rare clinical entity, may appear as a well-circumscribed mass or diffuse involvement of the pancreatic parenchyma. In case of diffuse pancreatic involvement the imaging findings may mimic acute pancreatitis, without clinical signs and symptoms, whereas, the presence of a well-circumscribed mass may mimic an adenocarcinoma (27, 28). The discrepancy between the lesion size and the absence of main pancreatic duct/common bile duct dilatation can be an important clue to the correct diagnosis. The absence of peripancreatic vessel invasion may also serve as a good indicator to the correct nature of the mass, rather than a pancreatic adenocarcinoma (27). Encasement of the vessels rather than luminal stenosis or occlusion is a common finding in lymphoma, due to the soft nature of the lymphomatous masses. These findings can also be revealed by CT, but they are not specific. In our experience, we strongly consider that the encasement of the fat may be a more reliable finding than the other findings stated previously. Nevertheless, unlike MRI, engulfed fat
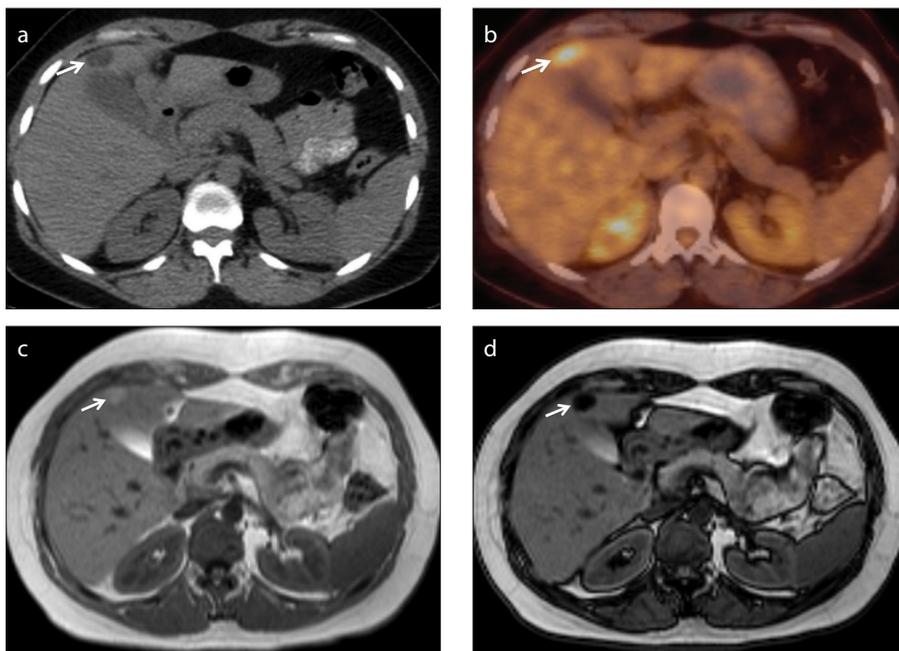
Figure 5. a–d. A 52-year-old female patient with renal cell carcinoma who underwent left partial nephrectomy. Axial PET-CT image **(a)** shows a hypodense nodular lesion *(arrow)* adjacent to gallbladder, with increased FDG uptake **(b,** *arrow)*, suspicious for metastasis. Lipid-rich hepatic adenoma is diagnosed by demonstration of fat on in-phase **(c)** and opposed-phase **(d)** MRI *(arrow)*.
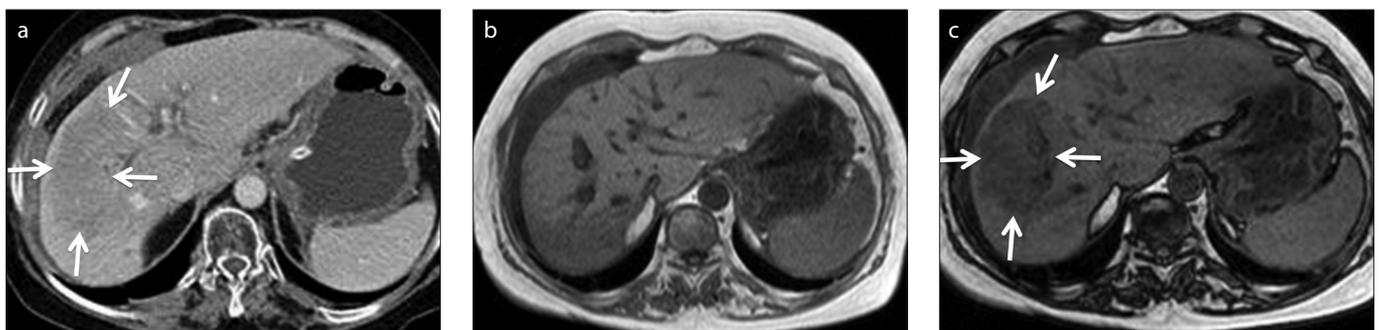
Figure 6. a–c. A 60-year-old female patient with right portal vein thrombosis. Contrast-enhanced axial CT image **(a)** shows parenchymal hypodensity *(arrows)* suspicious for a mass. In-phase **(b)** and opposed-phase **(c)** MRI demonstrate focal fat infiltration area *(arrows)*.

by the mass can be invisible on CT and may be detected as a nonspecific hypodense area within the mass, which may mimic the cystic/necrotic component of an adenocarcinoma (Fig. 11).

Musculoskeletal tissue

Fat containing musculoskeletal lesions are usually benign and the fat presence can be easily detected on CT, and sometimes even on US. However, that may not be the case in oncology patients as a new lesion should be treated as a metastatic focus, unless proven otherwise. In the differential diagnosis of a newly appearing mass in a cancer patient, a rare clinical entity, a Morel-Lavallée lesion should also be considered, especially in patients with a history of recent trauma (29). This entity refers to the traumatic separation of the skin from the subcutaneous tissue of the underlying muscular fascia with final formation of a cavity that may be filled with blood, lymph, or fat (29, 30). CT can be nondiagnostic as to the internal heterogeneity of the mass. However, with MRI the focal fat focus can be detected which is very helpful to reach the correct diagnosis (Fig. 12).

The conversion of red marrow to yellow (lipid rich) marrow is observed with increased age, and this finding can also be easily diagnosed by MRI (Fig. 13). Any process that replaces the lipid and hematopoietic components of the marrow, with no signal drop on the opposed-phase images should be approached as bone marrow infiltration, rather than conversion, until proven (31).

Peritoneum

Peritoneal invasion is commonly seen in patients with ovarian or gastric carcinoma as a result of tumor seeding. Known primary tumor and the classic appearance called omental cake are the key findings. Nevertheless, peritoneal and retroperitoneal space may rarely be invaded by myxoid liposarcoma (32, 33). CT may demonstrate the mass and its extension; however, further characterization is limited. In addition, CT appearance of myxoid liposarcoma may be confusing due to cyst-like appearance (32, 33). In fact, cystic appearance of myxoid liposarcoma is due to the lipid content invisible on CT. Thus, revealing fat content aids in diagnosis (Fig. 14).

Conclusion

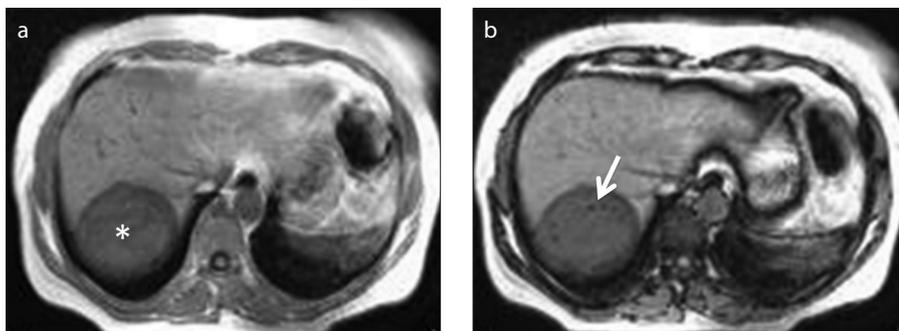Although CT can reveal small subcentimeter lesions thanks to its high spatial res-

Figure 7. a, b. A 30-year-old female patient with hydatid cyst of the liver *(asterisk)*. Opposed-phase MRI **(b)** shows fat droplets *(arrow)* within the cyst lumen as a result of biliary communication.
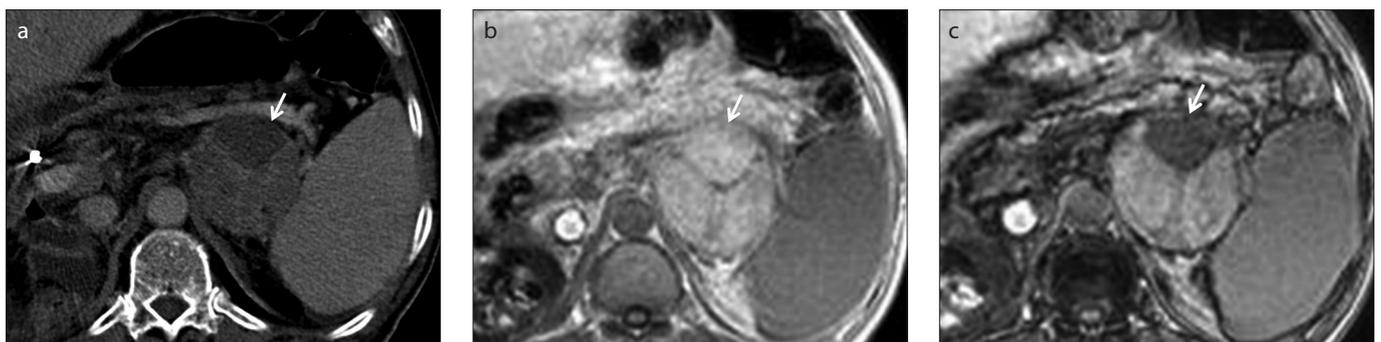

Figure 8. a–c. A 64-year-old male patient with metastatic hepatocellular carcinoma. Contrast-enhanced axial CT image **(a)** shows a heterogeneous left adrenal mass *(arrow)*. In-phase **(b)** and opposed-phase **(c)** MRI reveals fat content of the mass *(arrow)*, which was also seen in the primary tumor *(not shown)*.
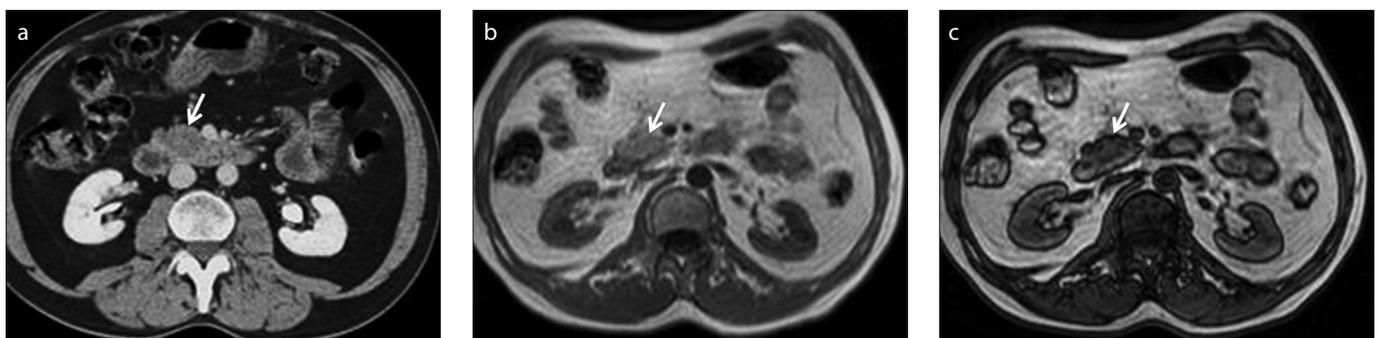

Figure 9. a–c. A 54-year-old male patient with a suspicious pancreatic mass. Contrast-enhanced axial CT image **(a)** shows a hypodense lesion *(arrow)* in uncinate process of the pancreas thought to be malignant. No discrete lesion is seen on in-phase MRI **(b,** *arrow)*. Focal fatty infiltration of the pancreas is revealed by decreasing signal intensity on opposed-phase image **(c,** *arrow)*.
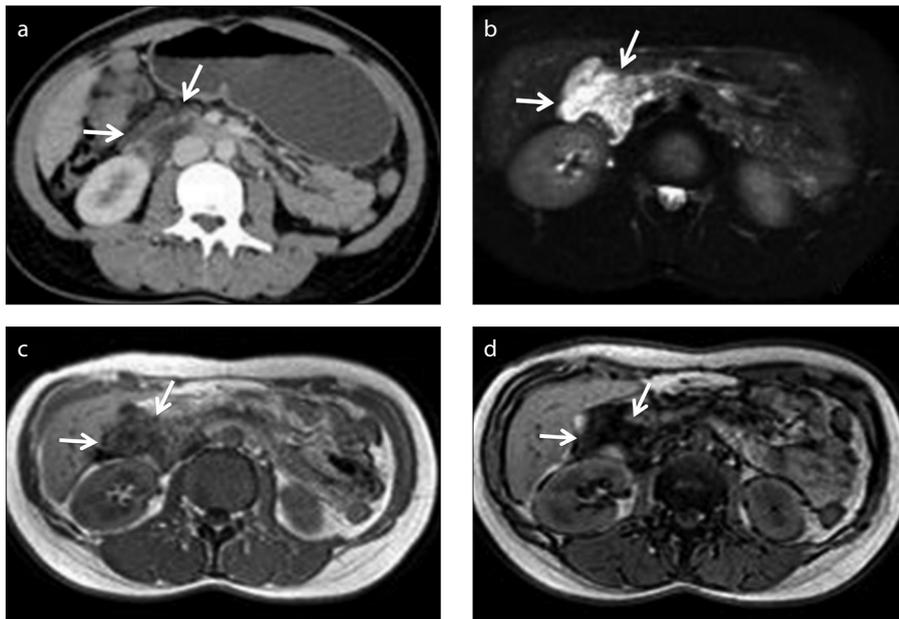
olution, further characterization of these small-sized abnormalities may not be done by CT. However, based on the accumulating clinical experience, it is now known that these subcentimeter hypodensities on CT may encompass invisible fat, which can be made visible by MRI. The demonstration of fat within a lesion is a helpful clinical finding that can potentially narrow the differential diagnosis and may significantly help the imaging specialist to reach the correct diagnosis.

Figure 10. a–d. A 38-year-old female patient with an incidentally detected peripancreatic mass. Contrast-enhanced axial CT image **(a)** shows a probably benign yet nonspecific cystic mass *(arrows)* adjacent to the head of the pancreas. Further characterization is limited on CT. Axial fat-suppressed T2-weighted image **(b)** clearly depicts cystic nature of the mass *(arrows)*. In-phase **(c)** and opposed-phase **(d)** MRI demonstrate fat content of the mass *(arrows)*, so that diagnosis of a peripancreatic lymphangioma can be made.
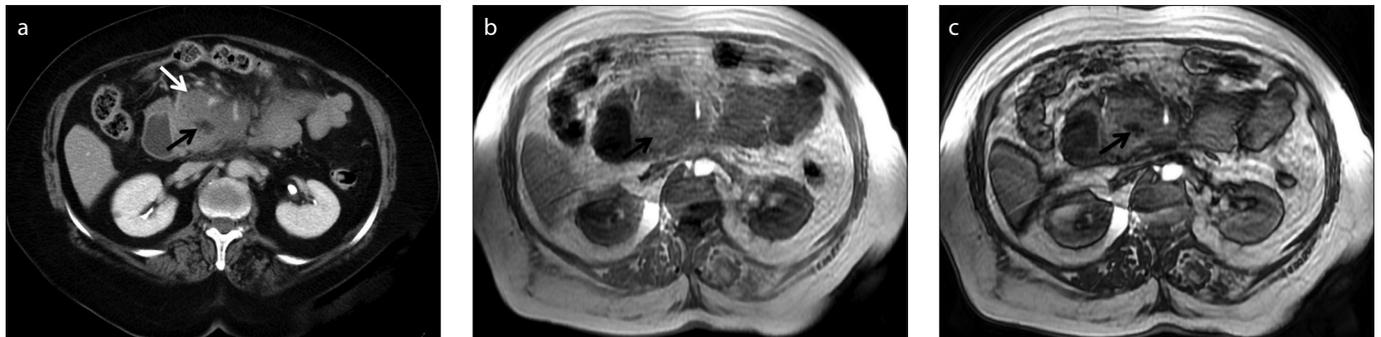

Figure 11. a–c. A 72-year-old previously healthy female patient with a pancreatic mass. Contrast-enhanced axial CT image **(a)** demonstrates a mass involving the uncinate process of the pancreas *(white arrow)*. Lack of vascular invasion is noted. A nonspecific hypodense lesion within the mass is also noted *(black arrow)* which is atypical for necrotic content. No further characterization can be made on CT. In-phase **(b)** and opposed-phase **(c)** MRI depicts fat *(black arrows)* within the mass. Diagnosis of pancreatic lymphoma was made histopathologically. Encasement rather than invasion of fat and vessels adjacent to mass, as well as lack of pancreatic duct dilatation are the clues for diagnosis.

Figure 12. a–c. A 49-year-old male patient with gastric carcinoma. Follow-up contrast-enhanced axial CT image **(a)** shows a new subcutaneous mass in the left upper thigh. Suspicious hypodensity thought to represent fat is also noted *(arrow)*. In-phase **(b)** and opposed-phase **(c)** MRI clearly show fat content *(arrows)*. Thus, diagnosis of Morel-Lavallée lesion can be made in a patient with a history of recent trauma.
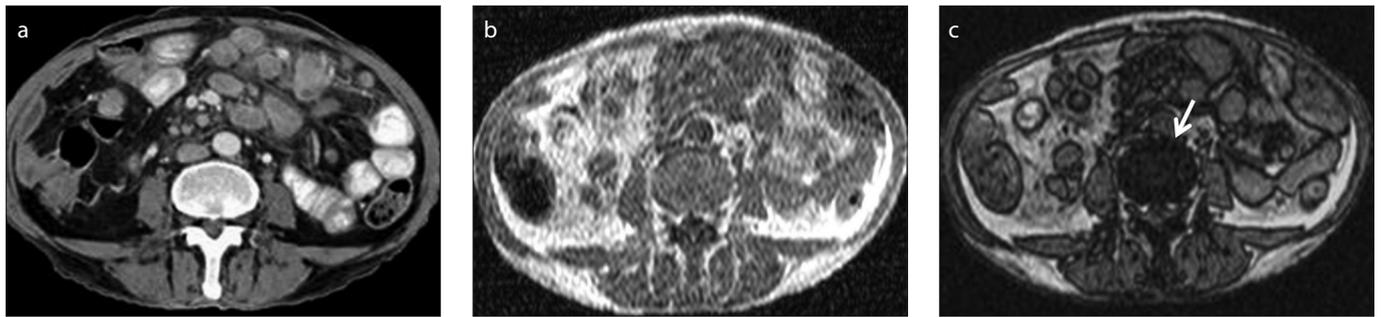
Figure 13. a–c. Conversion of red marrow to yellow (lipid rich) marrow. Contrast-enhanced axial CT image **(a)** shows a normal vertebral body. In-phase **(b)** and opposed-phase **(c)** MRI show signal drop *(arrow)* due to lipid content of yellow marrow. Preservation of signal drop excludes bone marrow infiltration.
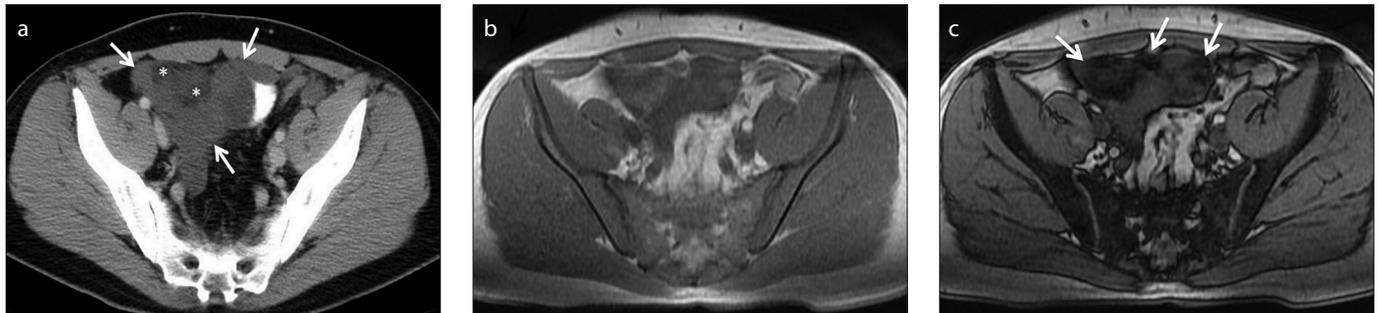

Figure 14. a–c. A 32-year-old male patient with myxoid liposarcoma metastatic to peritoneal space. Contrast-enhanced axial CT image **(a)** demonstrates more specifically the cystic nature (lower attenuation than muscle) and extension of the mass *(arrows)*. There is a suspicion of fat contents which are barely seen *(asterisks)*. Therefore, initial differential diagnosis is limited to cystic peritoneal masses. However crucial imaging finding was fat content of the mass, which was indistinct on CT. Fat content of the liposarcoma is revealed on in-phase **(b)** and opposed-phase **(c)** MRI *(arrows)*.

Conflict of interest disclosure

The authors declared no conflicts of interest.

References

1. Holalkere NS, Sahani DV, Blake MA, Halpern EF, Hahn PF, Mueller PR. Characterization of small liver lesions: Added role of MR after MDCT. J Comput Assist Tomogr 2006; 30:591–596. **[CrossRef]**
2. Mueller GC, Hussain HK, Carlos RC, Nghiem HV, Francis IR. Effectiveness of MR imaging in characterizing small hepatic lesions: routine versus expert interpretation. AJR Am J Roentgenol 2003; 180:673–680. **[CrossRef]**
3. Bottcher J, Hansch A, Pfeil A, et al. Detection and classification of different liver lesions: comparison of Gd-EOB-DTPA-enhanced MRI versus multiphasic spiral CT in a clinical single centre investigation. Eur J Radiol 2013; 82:1860–1869. **[CrossRef]**
4. Schwartz LH, Gandras EJ, Colangelo SM, Ercolani MC, Panicek DM. Prevalence and importance of small hepatic lesions found at CT in patients with cancer. Radiology 1999; 210:71–74. **[CrossRef]**
5. Delfaut EM, Beltran J, Johnson G, Rousseau J, Marchandise X, Cotten A. Fat suppression in MR imaging: techniques and pitfalls. Radiographics 1999; 19:373–382. **[CrossRef]**
6. Bley TA, Wieben O, Francois CJ, Brittain JH, Reeder SB. Fat and water magnetic resonance imaging. J Magn Reson Imaging 2010; 31:4–18. **[CrossRef]**
7. Pokharel SS, Macura KJ, Kamel IR, Zaheer A. Current MR imaging lipid detection techniques for diagnosis of lesions in the abdomen and pelvis. Radiographics 2013; 33:681–702. **[CrossRef]**
8. Earls JP, Krinsky GA. Abdominal and pelvic applications of opposed-phase MR imaging. AJR Am J Roentgenol 1997; 169:1071–1077. **[CrossRef]**
9. Basaran C, Karcaaltincaba M, Akata D, et al. Fat-containing lesions of the liver: cross-sectional imaging findings with emphasis on MRI. AJR Am J Roentgenol 2005; 184:1103–1110. **[CrossRef]**
10. Dixon WT. Simple proton spectroscopic imaging. Radiology 1984; 153:189–194. **[CrossRef]**
11. Ma J. Dixon techniques for water and fat imaging. J Magn Reson Imaging 2008; 28:543–558. **[CrossRef]**
12. Fultz PJ, Hampton WR, Skucas J, Sickel JZ. Differential diagnosis of fat-containing lesions with abdominal and pelvic CT. Radiographics 1993;13:1265–1280. **[CrossRef]**
13. Yoshikawa J, Matsui O, Takashima T, et al. Focal fatty change of the liver adjacent to the falciform ligament: CT and sonographic findings in five surgically confirmed cases. AJR Am J Roentgenol 1987; 149:491–494. **[CrossRef]**
14. Robinson PJ. The effects of cancer chemotherapy on liver imaging. Eur Radiol 2009; 19:1752–1762. **[CrossRef]**
15. Chung KY, Mayo-Smith WW, Saini S, Rahmouni A, Golli M, Mathieu D. Hepatocellular adenoma: MR imaging features with pathologic correlation. AJR Am J Roentgenol 1995; 165:303–308. **[CrossRef]**
16. Prasad SR, Wang H, Rosas H, et al. Fat-containing lesions of the liver: radiologic-pathologic correlation. Radiographics 2005; 25:321–331. **[CrossRef]**
17. Marn CS, Francis IR. CT of portal venous occlusion. AJR Am J Roentgenol 1992; 159:717–726. **[CrossRef]**
18. Mendez Montero JV, Arrazola Garcia J, Lopez Lafuente J, Antela Lopez J, Mendez Fernandez R, Saiz Ayala A. Fat-fluid level in hepatic hydatid cyst: a new sign of rupture into the biliary tree? AJR Am J Roentgenol 1996; 167:91–94. **[CrossRef]**
19. Honigschnabl S, Gallo S, Niederle B, et al. How accurate is MR imaging in characterization of adrenal masses: update of a long-term study. Eur J Radiol 2002; 41:113–122. **[CrossRef]**
20. Mayo-Smith WW, Boland GW, Noto RB, Lee MJ. State-of-the-art adrenal imaging. Radiographics 2001; 21:995–1012. **[CrossRef]**
21. Yasaka K, Gonoi W, Akai H, et al. Differentiation of adrenal tumors in patients with hepatocellular carcinoma: adrenal adenoma versus metastasis. Eur J Radiol 2013; 82:1213–1218. **[CrossRef]**
22. Kim HJ, Byun JH, Park SH, et al. Focal fatty replacement of the pancreas: usefulness of chemical shift MRI. AJR Am J Roentgenol 2007; 188:429–432. **[CrossRef]**
23. Matsumoto S, Mori H, Miyake H, et al. Uneven fatty replacement of the pancreas: evaluation with CT. Radiology 1995; 194:453–458. **[CrossRef]**
24. Koenig TR, Loyer EM, Whitman GJ, Raymond AK, Charnsangavej C. Cystic lymphangioma of the pancreas. AJR Am J Roentgenol 2001; 177:1090. **[CrossRef]**
25. Schneider G, Seidel R, Altmeyer K, et al. Lymphangioma of the pancreas and the duodenal wall: MR imaging findings. Eur Radiol 2001; 11:2232–2235. **[CrossRef]**
26. Choi JY, Kim MJ, Kim JH, et al. Solid pseudopapillary tumor of the pancreas: typical and atypical manifestations. AJR Am J Roentgenol 2006; 187:W178–186. **[CrossRef]**

27. Merkle EM, Bender GN, Brambs HJ. Imaging findings in pancreatic lymphoma: differential aspects. AJR Am J Roentgenol 2000; 174: 671–675. **[CrossRef]**

28. Van Beers B, Lalonde L, Soyer P, et al. Dynamic CT in pancreatic lymphoma. J Comput Assist Tomogr 1993; 17:94–97. **[CrossRef]**

29. Hak DJ, Olson SA, Matta JM. Diagnosis and management of closed internal degloving injuries associated with pelvic and acetabular fractures: the Morel-Lavallee lesion. J Trauma 1997; 42:1046–1051. **[CrossRef]**

30. Hudson DA, Knottenbelt JD, Krige JE. Closed degloving injuries: results following conservative surgery. Plast Reconstr Surg 1992; 89:853–855. **[CrossRef]**

31. Disler DG, McCauley TR, Ratner LM, Kesack CD, Cooper JA. In-phase and out-of- phase MR imaging of bone marrow: prediction of neoplasia based on the detection of coexistent fat and water. AJR Am J Roentgenol 1997; 169:1439–1447. **[CrossRef]**

32. Benjaminov O, Gutman H, Nyabanda R, Keinan R, Sabach G, Levavi H. Myxoid liposarcoma: an unusual presentation. AJR Am J Roentgenol 2007; 188:817–821. **[CrossRef]**

33. Kim T, Murakami T, Oi H, et al. CT and MR imaging of abdominal liposarcoma. AJR Am J Roentgenol 1996; 166:829–833. **[CrossRef]**